Probing the influence of inertia, viscosity, and initial offset on the hydrodynamic interaction of droplet pairs in confined shear flow

S. M. Abdullah Al Mamun and Samaneh Farokhirad*
Department of Mechanical and Industrial Engineering, New Jersey Institute of Technology, Newark, New Jersey 07114, USA

(Received 26 May 2022; accepted 7 December 2022; published 22 December 2022)

Understanding the hydrodynamics of droplet collision is vitally important due to the inherent small-scale phenomena and various practical applications. The morphology, course trajectory, and final state of the droplets in such a collision are greatly affected by different physical parameters together with system geometry. Yet the collision behavior of droplet pairs at high density and viscosity ratios remains unexplored and unquantified, and therefore the critical density and viscosity ratios for the collision mode of droplets under geometric parameters were unknown. Through computational analyses, we address the interplay between the density ratio (60 to 800), the viscosity ratio (24 to 60), the initial offset, and the confinement on the coalescence of droplet pairs subjected to a confined shear flow. Simulations have been performed using a free-energy-based lattice Boltzmann method, with the aim of determining new regimes compared to the previous study. The results reveal that the coupling effect of density ratios and viscosity ratios contributes to generating inertia and viscous interaction forces that significantly impact the coalescence consequences. On the other hand, the wall confinement and the initial vertical offset of droplets are shown to play a significant role in either promoting or suppressing the collision mode of interacting droplets. Interestingly, we observe unusual trajectory motion of droplets for an intermediate range of density ratios (i.e., 245–600) near the critical initial offset of droplets. Regions of different collision modes are further presented in terms of phase diagrams, which reveal the critical dependency of droplet behavior on the coupling effect of density ratios, viscosity ratios, initial vertical offset, and confinement. The reported results are expected to provide new insights into the collision of pair droplets under confined shear flows in the effect of various parameters and help elucidate the intrinsic nature and the condition of coalescence.

DOI: 10.1103/PhysRevFluids.7.123603

I. INTRODUCTION

Multiphase and multiscale fluid flow phenomena are ubiquitous in nature and have a diverse range of real-life applications. One of such cases encountered frequently is dispersed fluid droplets in another matrix fluid. This type of hydrodynamic interaction between two immiscible fluids is central to the wide applications in microfluidics [1–4], pharmaceutics [5,6], drug delivery [7,8], polymer blending [9–11], emulsification [12–14], and enhanced oil recovery [15,16] to name a few. Resolving such dynamic interactions through simulation is challenging due to the small-scale activities especially occurring at the interface regions that ultimately influence the large-scale consequences over the droplets. Thus, the study of the conditions behind droplet coalescence and its behavior in the effects of various parameters has been of paramount importance.

*samaneh.farokhirad@njit.edu

Typically, the coalescence process can be described in three stages [17]. First, the droplets approach each other from their initial location. Once they come into collision, the matrix fluid film between them starts thinning out, and this is the second phase, called film drainage. As the film thickness continues to decrease, at some point, two droplet surfaces come close enough that the intermolecular forces dominate, destabilizing the film and causing film rupture. Eventually, the droplets coalesce with each other.

The outcome of such interactions is not only determined by the properties of the material component or concentration but also by the droplet size distribution. Different physical parameters (such as density ratio and viscosity ratio of droplets to the matrix fluid), as well as geometric parameters (such as confinement and initial offset between droplets), play important roles in coalescence dynamics. Depending on the interplay of these parameters, different collision modes appear, including the reverse back of droplets from the direction of initial movement caused by shear drag, merging (i.e., coalescence), and passing over one another [18,19]. All of these factors motivate the research of understanding and predicting the hydrodynamics of deformable droplets based on flow conditions.

Several authors have studied the coalescence and collision mode of droplets subjected to a confined shear flow using both computational and experimental approaches [20–27]. Guido and Simone [20] used video-enhanced contrast optical microscopy to investigate the collision of two equal-sized droplets immersed in an immiscible liquid subjected to a shear flow. Their study was confined to a small range of viscosity ratio (0.36–1.4) while keeping the density ratio fixed and close to 1. They showed that the vertical offset distance tends to increase irreversibly after the collision, which presents a droplet dispersion mechanism in such a system. Shardt and coworkers [21] simulated droplet collisions in shear flows using a free-energy-based lattice Boltzmann method (LBM) to quantify the effects of the droplet size relative to the interface thickness, the Peclet number, the confinement, and the vertical offset on the critical capillary number (Ca), while keeping the density and viscosity ratios fixed at 1.

Huang and Liang [22] simulated the collision and coalescence of three-dimensional (3D) droplets in a confined shear flow using the phase-field-based LBM. They focused on a two-phase system with equal density and viscosity fluids and explored the coupling effect of Ca and Reynolds (Re) numbers, while keeping the offset and confinement fixed. Three types of droplet behaviors were identified: coalescence, break-up after coalescence, and noncoalescence. In the lower Re region, droplets show all three patterns of collision outcome depending on the Ca numbers. In contrast, one critical Ca number was encountered in the intermediate Re range that characterizes the flow transition from coalescence to noncoalescence. Finally, for a sufficiently large value of Re number, the droplets were observed to slide over each other, irrespective of Ca variation.

The effect of geometrical confinement and vertical offset was studied experimentally by Bruyn *et al.* [18] for both bulk and confined conditions. The polymers they used in their experiment for the droplet phase and the matrix fluid have a viscosity ratio of 0.095 and a density ratio of about 1. The confinement seemed to play a significant role in coalescence conditions, and the possibility of droplets' coalescence at larger initial offsets was mainly attributed to the effect of confinement. Results with different initial offsets on the velocity gradient direction indicate a higher critical initial offset above which coalescence is impossible. A lower critical initial offset below which bounce back and reverse trajectory motion of the droplets are also found. To evaluate the effect of viscosity ratio along with the geometrical confinement, another experimental study was performed by Bruyn *et al.* [19]. For each of the systems of three different droplet materials paired with a Newtonian matrix resulting in three different viscosity ratios (0.1, 1.1, and 2.6), confinement leads to an increase of the critical Ca number and supports possible coalescence with higher initial offset.

The effect of wall confinement in promoting the coalescence of droplets with unit viscosity and density ratios was also observed by Chen *et al.* [23] in their experimental investigation. They noticed that the parallel walls play an important role and induce changes in the interaction of droplets. In contrast, sufficiently confined walls produce force comparable to a hydrodynamic force influencing the drainage of the film between two approaching droplets.

Chen and coworkers [24] explored the behavior of two interactive circular droplets in a confined shear flow and their hydrodynamic interaction based on a computational fluid dynamics simulation employing the volume-of-fluid method. Two types of droplet behaviors are experienced during their interaction. Increased confinement causes the droplets to transit from pass-over toward the reverse-back motion governed by the presiding role of the entrainment of the reversing-flow matrix fluid. On the other hand, the enlarged initial separation results in the emergence of pass-over motion. In addition, the combined effects of confinement, Re, and Ca on the deformation of droplets and their trajectories were investigated. However, how changing the density and viscosity ratios influences the collision outcome of droplets remains unconsidered.

Sarkar *et al.* [25] showed that the inertia-less Stokes flow governs small-size droplets with small velocities in microcirculatory flows bounded by walls. Instead of adopting free streamlines with a finite cross-stream, which is common in free shear, their simulation found that the droplets move toward the centerline, maintaining a zero cross-stream separation but simultaneously with a net streamwise separation.

The collision of droplet pairs in an immiscible fluid matrix under shear flow was simulated by Bayareh *et al.* [26], solving the full Navier-Stokes equation by a front-tracking method. The effect of varying different geometric parameters and viscosity ratio (0.19–1.2) while keeping the density ratio constant at one was studied in their simulations. Close observation was made on the time evolution of the distance between droplet centers along the velocity gradient direction.

Finally, the effects of Ca number and viscosity ratio (0.25–8) on the cross-flow self-diffusion coefficients for rigid and deformable droplets undergoing simple shear flow were studied by Loewenberg and Hinch [27] using the boundary integral method. Their results show that, while keeping the density ratio fixed at one, the self-diffusivities of droplets depend strongly on the viscosity ratio and moderately on the Ca number.

Despite numerical and experimental studies on the motion trajectories, droplet morphologies, regime of interactions, and the influence parameters (such as vertical offset of droplets, wall confinement, and viscosity ratio), the role of inertia on the dynamic evolution and collision mode of droplets has not been addressed. Additionally, most of the earlier works have been done for a smaller range of viscosity ratios, basically ranging from 0.1 to 8. Therefore, the objectives of the present work are to provide results of droplet collision over a large range of density ratios (60–800), extend previous results to a wider range of viscosity ratios (24–60), and determine new regimes under collaborative roles of vertical offset, confinement, density ratio, and viscosity ratio. In the present work, we conduct our investigation using numerical simulations, applying a proposed LBM [28,29], which is based on the Chan-Hilliard diffuse interface theory for binary fluids. Compared to the LBM used in previous numerical investigations on the coalescence of pair droplets in a shear flow [21,22], the present LBM is capable of eliminating the parasitic currents and consequently can accommodate higher density and viscosity ratios between the fluid components [30–33]. We have investigated the effect of inertia and viscous forces on droplet coalescence in a systematic way for a range of wall confinement and initial offset between the droplets.

The rest of the manuscript is organized as follows. In Sec. II, we briefly review the methods and formulation of the algorithm required to perform the simulation of the studied phenomena. In Sec. III, we present validation of the adopted algorithm and discuss the results received from our analysis. This is followed by a summary of major conclusions from this study in Sec. IV.

II. METHOD

In the free-energy-based LBM for binary fluid, one follows the evolution of two discrete density distributions, g_α and h_α, to model hydrodynamics and the evolution of phase-field, respectively. In this study, we apply the LBM proposed by Lee and Liu [28], which is developed based on the Cahn-Hilliard diffuse interface theory for binary fluids to study droplet coalescence in confined shear flow. We will be establishing a brief overview of the method here; for more details on the theory and method, readers are referred to Refs. [29,34–37]. The LBM follows a two-step approach

to solve advection-diffusion equations. In the first step, known as the streaming step, the density distribution functions at each lattice node are propagated to adjacent nodes along with a set of discrete velocities $\mathbf{e}_\alpha$ where α identifies the discrete direction. There are several models of lattice arrangement depending on the dimensional space of the simulation and the number of linkages used for the information propagation. For our case study, we will be adopting the D2Q9 model of lattice, where D2 denotes a two-dimensional domain and Q9 refers to the speed model with nine linkages or directions. The second step of LBM, known as the collision step, determines the effect of collisions between molecules leading the density distribution function toward an equilibrium distribution by relaxing them at each node. A scalar order parameter C (i.e., composition) is introduced, which satisfies the following convective Cahn-Hilliard equation [28]:

$$\frac{\partial C}{\partial t} + \mathbf{u} \cdot \nabla C = M \nabla^2 \mu_c, \tag{1}$$

which involves mobility parameter M and chemical potential μ_c. Among the two distribution functions g_α and h_α, the former is used for the calculation of pressure and momentum of the two-component mixture, and the latter is used as a phase-field function for the transport of the composition. These two distribution functions evolve according to following equations [28]:

$$\frac{\partial g_\alpha}{\partial t} + \mathbf{e}_\alpha \cdot \nabla g_\alpha = -\frac{1}{\lambda}(g_\alpha - g_\alpha^{\mathrm{eq}}) + (\mathbf{e}_\alpha - \mathbf{u}) \cdot \left\{ \nabla \rho c_s^2 [\Gamma_\alpha - \Gamma_\alpha(0)] + \mu_c \nabla C \Gamma_\alpha \right\}, \tag{2}$$

$$\frac{\partial h_\alpha}{\partial t} + \mathbf{e}_\alpha \cdot \nabla h_\alpha = -\frac{1}{\lambda}(h_\alpha - h_\alpha^{\mathrm{eq}}) + M \nabla^2 \mu_c \Gamma_\alpha + (\mathbf{e}_\alpha - \mathbf{u}) \cdot \left[\nabla C - \frac{C}{\rho c_s^2}(\nabla p - \mu_c \nabla C) \right] \Gamma_\alpha, \tag{3}$$

where the equilibrium distribution functions are defined as

$$g_\alpha^{\mathrm{eq}} = t_\alpha \left\{ p + \rho c_s^2 \left[\frac{\mathbf{e}_\alpha \cdot \mathbf{u}}{c_s^2} + \frac{(\mathbf{e}_\alpha \cdot \mathbf{u})^2}{2c_s^4} - \frac{\mathbf{u} \cdot \mathbf{u}}{2c_s^2} \right] \right\}, \tag{4}$$

$$h_\alpha^{\mathrm{eq}} = t_\alpha C \left[1 + \frac{\mathbf{e}_\alpha \cdot \mathbf{u}}{c_s^2} + \frac{(\mathbf{e}_\alpha \cdot \mathbf{u})^2}{2c_s^4} - \frac{\mathbf{u} \cdot \mathbf{u}}{2c_s^2} \right]. \tag{5}$$

In the above equations, $\mathbf{e}_\alpha$ is the microscopic particle velocity in the α direction, $\mathbf{u}$ is the volume-averaged velocity, c_s is the lattice speed of sound, ρ is the mixture density, p is the dynamic pressure, λ is the relaxation time, t_α is the weighting factor, and Γ_α is defined as $\Gamma_\alpha = \Gamma_\alpha(\mathbf{u}) = h_\alpha^{\mathrm{eq}}/C$. The dimensionless relaxation time $\tau = \lambda/\delta t$ is related to the kinematic viscosity by $\nu = \tau c_s^2 \delta t$. The density can be related to the composition using the following linear function [28]:

$$\rho = C\rho_1 + (1 - C)\rho_2, \tag{6}$$

where ρ_1 and ρ_2 are the bulk densities of two fluids. The chemical potential, μ is defined as the derivative of the free energy with respect to the order parameter, and the free energy is given by [37]

$$E(C) = E_0(C) + \frac{\kappa}{2}|\nabla C|^2, \tag{7}$$

where $E(C)$ is the total free energy, $E_0(C)$ is the free energy density of the binary solution, ∇C is the composition gradient, and κ is the gradient parameter related to the surface tension of the interface between two phases. The free energy density is taken as $E_0(C) = \beta C^2 (C-1)^2$ [28] with β being a constant. The equilibrium profile and surface tension of the interface in equilibrium can be determined by minimizing the mixing energy. The plane interface profile at equilibrium is then evaluated as [28]

$$C(z) = \frac{1}{2} + \frac{1}{2}\tanh\left(\frac{2z}{\xi}\right), \tag{8}$$

where z denotes the coordinate normal to the interface plane and ξ is the interface thickness. Once the surface tension and interface thickness are chosen, β and κ are specified as $\beta = 12\sigma/\xi$ and $\kappa =$

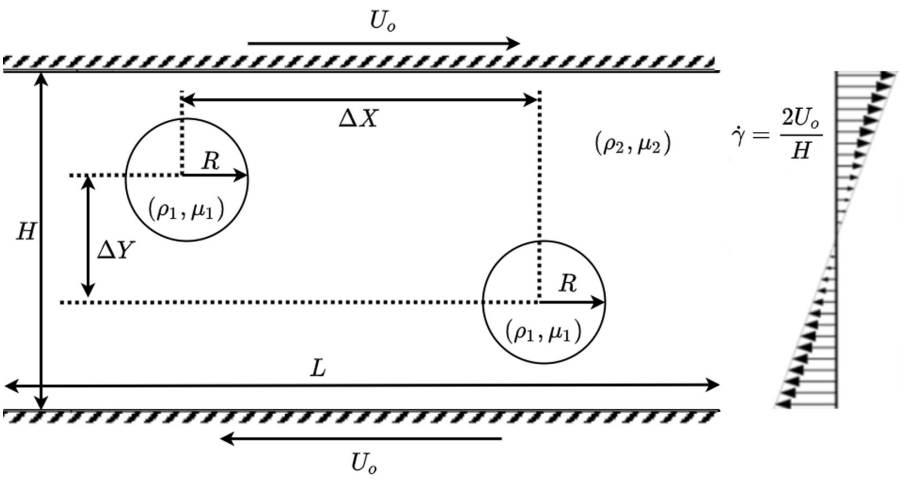

FIG. 1. Schematic representation of a droplet pair with an initial radius of R in a confined shear flow. The droplets are located between two parallel plates that are a distance H apart and move in opposite directions. ΔX and ΔY are the horizontal and vertical distances between the centers of the droplets.

$\beta\xi^2/8$. Finally, the macroscopic variables such as composition, momentum, and dynamic pressure can be obtained by taking the moments of h_α and g_α:

$$C = \sum_\alpha h_\alpha, \tag{9}$$

$$\rho \mathbf{u} = \frac{1}{c_s^2} \sum_\alpha \mathbf{e}_\alpha g_\alpha, \tag{10}$$

$$p = \sum_\alpha g_\alpha. \tag{11}$$

For detailed discretization of Eqs. (2) and (3) and boundary conditions, readers are referred to Ref. [28].

III. RESULTS

A. Validation

A schematic two-dimensional representation for the coalescence of droplet pairs in a confined shear flow is demonstrated in Fig. 1. Two spherical droplets, both of radius R, are initially separated by a horizontal spacing of ΔX and a vertical distance of ΔY as measured between their centers. The simple shear flow is generated by the motion of the top and bottom walls with a shear rate of $\dot{\gamma} = 2U_o/H$, where U_o is the horizontal speed of the planes as indicated in Fig. 1, and H is the vertical spacing between them. Other parameters that define the physical problem are the densities of the droplet (ρ_1) and matrix fluid (ρ_2), the dynamic viscosities of the droplet (μ_1) and matrix fluid (μ_2), and the surface tension (σ) between the droplet and matrix fluid. Since the scale of droplets in our analysis is much smaller than the capillary length (i.e., $\sqrt{[\sigma/(\Delta\rho g)]}$), the gravity force is neglected.

The dimensionless parameters related to the coalescence of pair droplets under confined shear flow are the density ratio $\rho_{12} = \rho_1/\rho_2$, the viscosity ratio $\mu_{12} = \mu_1/\mu_2$, the confinement ratio $2R/H$ (ratio of droplet diameter to gap spacing), Reynolds number $\mathrm{Re} = \frac{\rho_2 \dot{\gamma} R^2}{\mu_2}$, Capillary number $\mathrm{Ca} = \frac{\mu_2 \dot{\gamma} R}{\sigma}$ (the ratio of viscous force to surface tension force), and Weber number $\mathrm{We} = \frac{\rho_2 \dot{\gamma} R^3}{\sigma}$ (the ratio of inertia force to surface tension force). Since the Weber number and the Capillary

TABLE I. Simulation parameters and their values.

Parameter	Definition	Value
	Dimensionless parameters	
Reynolds number	$\mathrm{Re} = \frac{\rho_2 \dot{\gamma} R^2}{\mu_2}$	1.0
Capillary number	$\mathrm{Ca} = \frac{\mu_2 \dot{\gamma} R}{\sigma}$	0.01
Weber number	$\mathrm{We} = \mathrm{ReCa} = \frac{\rho_2 \dot{\gamma} R^3}{\sigma}$	0.01
Confinement	$\frac{2R}{H}$	0.30–0.39
Vertical offset	$\frac{\Delta Y}{2R}$	0.04–1.04
Horizontal separation	$\frac{\Delta X}{2R}$	1.26
Density ratio	$\rho_{12} = \frac{\rho_1}{\rho_2}$	60–800
Viscosity ratio	$\mu_{12} = \frac{\mu_1}{\mu_2}$	24–60
	Numerical parameters	
Dimensionless mobility	$S = \frac{\sqrt{M\mu_1}}{R}$	0.004
Interface thickness	ξ	4 lattice units

number are related by $\mathrm{We} = \mathrm{ReCa}$, only one of them has been considered in the present study. Other geometric parameters are vertical offset and horizontal distance between droplets defined as $\frac{\Delta Y}{2R}$ and $\frac{\Delta X}{2R}$, respectively. The numerical mobility, M, represents a parameter that is absent from the physical parameter list but nevertheless plays an important role in the simulations as it determines the rate of Cahn-Hilliard diffusion. An appropriate dimensionless number that can characterize the effect of the mobility is $S = \sqrt{(M\mu_1)}/R$ [38]. A summary of the detailed parameter set is provided in Table I along with their values considered in this work.

To validate our results, we first conduct numerical experiments for three different Ca numbers and compare the time evolution of droplet collision with the numerical simulation performed in [21]. The top rows of Figs. 2(a), 2(b) and 2(c) show results from previous work [21], while the bottom rows of Figs. 2(a), 2(b) and 2(c) demonstrate results obtained from our simulation of droplet's evolution on collision for the same Ca numbers. Our simulation experiments were performed with the same dimensionless parameters as in Ref. [21], i.e., $\Delta X/2R = 1.26$, $\Delta Y/2R = 0.86$, $2R/H = 0.39$, and $\mathrm{Re} = 1$. The results of the current study on the evolution of droplets on collision display great agreement with those observed by Shardt *et al.* [21].

From the final two frames, it can be noticed that the droplets coalesce only for $\mathrm{Ca} = 0.08$, and they get separated for $\mathrm{Ca} = 0.09$ and 0.1. We must point out that although qualitative behavior of the 2D and 3D systems is generally found to agree, some differences in the neck formation and inclination angle can be visualized due to the differences in the drainage of the 2D versus 3D thin fluid film separating the two droplets.

We also examine the sensitivity of our results in Fig. 2(c) to the mesh resolution by repeating the calculations using systematically refined grids with three different grid resolutions, 164×82, 328×164, and 656×328 corresponding to droplet radius of 16, 32, and 64 lattice units, respectively, while keeping the interface thickness fixed at four lattice units. Figure 3(a) presents the evolution of vertical offset as a function of horizontal separation for those three different resolutions. It can be seen that the result on the 328×164 mesh resolution does not exhibit any significant difference from the results on the finer one (656×328). The result from the smallest resolution considered here (164×82) shows a little deviation from the other two. The critical snapshots of droplet deformation throughout the evolution from all three resolutions have been illustrated in Fig. 3(b), confirming the independency of results for the mesh resolution 328×164 and beyond. Thus, the channel with a mesh size of 328×164 is considered for the rest of our study and analysis.

Generally speaking, to approach the sharp interface limit, the interface thickness ξ should be small relative to other length scales L of the problem. This parameter can be characterized by the Cahn number $\mathrm{Cn} = \frac{\xi}{L} \ll 1$ [38]. When the droplet radius (i.e., $R = 16, 32,$ and 64 lattice units)

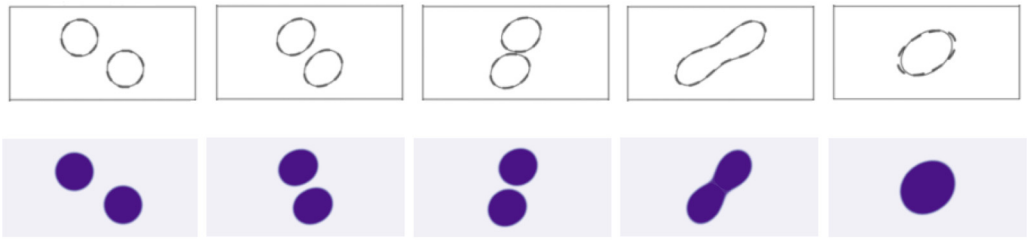

(a) Ca=0.08

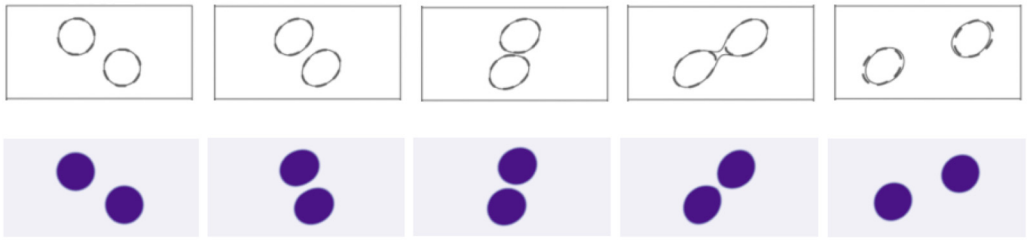

(b) Ca=0.09

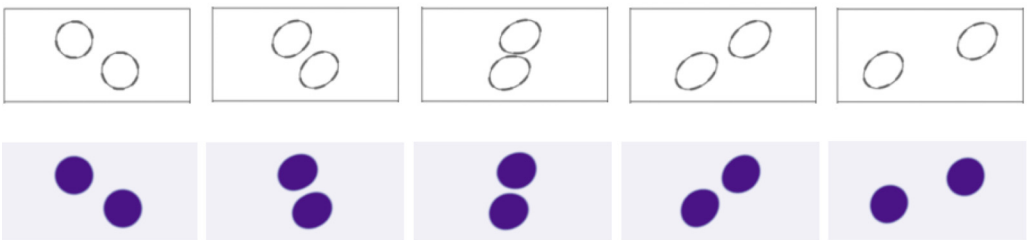

(c) Ca=0.10

FIG. 2. Comparison and validation of the adopted LBM algorithm with previous simulation results from Ref. [21] for a pair of droplets in confined shear flow with three different capillary numbers. The parameter values for the simulations are Re $= 1.0$, $\Delta X/2R = 1.26$, $\Delta Y/2R = 0.86$, $2R/H = 0.39$, and $\rho_{12} = \mu_{12} = 1.0$. The top rows of (a)–(c) show results from Ref. [21], while the bottom rows of (a)–(c) demonstrate results obtained from current work.

is chosen as the length scale, Cn $= 0.25, 0.125,$ and 0.0625, respectively, as the resolution is increased. However, we must note that when using a diffuse interface method for the coalescence of droplets, nonzero interface thickness (i.e., Cn) and diffusivity (i.e., S) are required for droplets to merge into a single droplet [39]. In this case, the ratio of interfacial thickness to the droplet size (Cn) must be large enough to avoid any delay in the coalescence due to an increased time for the film drainage but small enough to avoid fast coalescence. In our simulation, we found Cn $= 0.125$ as a sufficient finite value to simulate a physical system in which droplets coalesce during the time of the collision. On the other hand, the interfacial mobility M has to be adjusted carefully such that it is large enough to keep the interface near its equilibrium state but small enough to minimize damping near the interface [40]. Following the scaling argument, $S \approx \mathrm{Cn}^0$ suggested by Yue *et al.* [38], the effect of mobility has been studied by changing S from 0.00096 to 0.011 while keeping all other parameters, including Cn fixed. From Fig. 4(a), it can be noticed that varying S from 0.00096 to

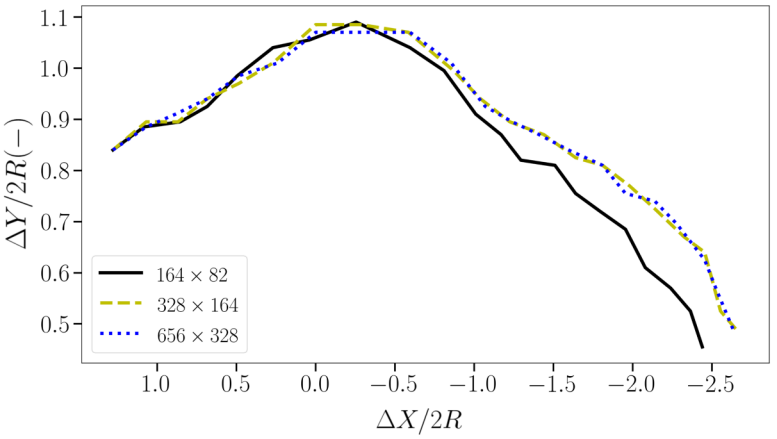

(a) Evolution of vertical offset as a function of horizontal separation.

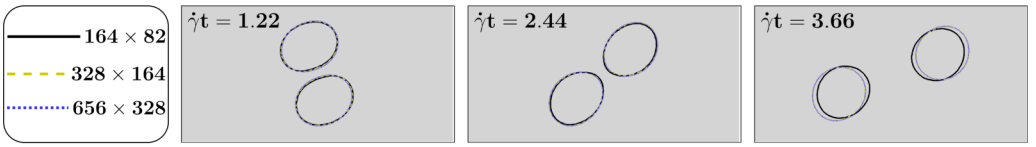

(b) Time-lapse images of droplet shape.

FIG. 3. Grid dependency test for the simulation case with Re $= 1.0$, Ca $= 0.10$, $\Delta X/2R = 1.26$, $\Delta Y/2R = 0.86$, $2R/H = 0.39$, and $\rho_{12} = \mu_{12} = 1.0$.

0.0054 results in a slight change in the evolution of pair droplets before (i.e., $\dot{\gamma}t = 4.27$) and after coalescence (i.e., $\dot{\gamma}t = 24.4$). For more clarification, the horizontal and vertical offsets of droplets at $\dot{\gamma}t = 4.27$ are provided in Fig. 4(b). Therefore, in the simulation, we have used $S = 0.004$, for which our results become independent of the mobility parameter.

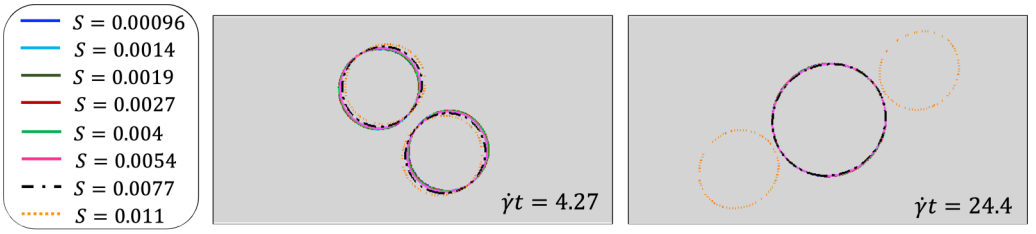

(a) Time-lapse images of interface shape for various dimensionless mobility parameters.

S	0.00096	0.0014	0.0019	0.0027	0.004	0.0054	0.0077	0.011
$\frac{\Delta x}{R}$	1.74	1.73	1.73	1.73	1.74	1.66	1.69	1.42
$\frac{\Delta y}{R}$	−1.58	−1.6	−1.6	−1.63	−1.62	−1.66	−1.6	−1.86

(b) Report of the values of vertical and horizontal offsets at $\dot{\gamma}t = 4.27$.

FIG. 4. Effect of interfacial mobility on the evolution of the droplets before and after coalescence.

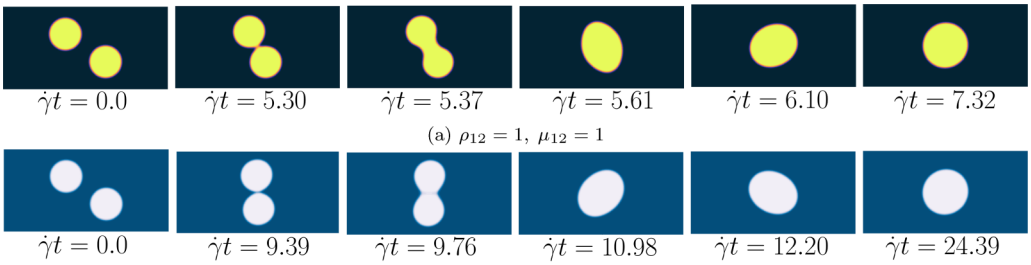

(a) $\rho_{12} = 1,\ \mu_{12} = 1$

(b) $\rho_{12} = 800,\ \mu_{12} = 60$

FIG. 5. Demonstration of coalescence behavior for the two marginal cases [(a) $\rho_{12} = 1,\ \mu_{12} = 1$ and (b) $\rho_{12} = 800,\ \mu_{12} = 60$] explored among all the density ratio and viscosity ratio combination of this study with Re $= 1.0$, Ca $= 0.01$, We $= 0.01$, $\Delta X/2R = 1.26$, $\Delta Y/2R = 0.86$, and $2R/H = 0.39$.

B. Effect of density and viscosity ratios

To explore the effect of inertial and viscous forces on the coalescence behavior, we have conducted simulations for a combination of different density ratios and viscosity ratios. To initiate our observation, first, we consider coalescence evolution for the two extreme cases ($\rho_{12} = 1,\ \mu_{12} = 1$ and $\rho_{12} = 800,\ \mu_{12} = 60$), and critical snapshots have been displayed as contour plots in Fig. 5. It can be observed that the density and viscosity ratios have substantial effects on the coalescence progression where the droplets are found to behave differently in terms of advancement to coalescence timing. It can also been noticed that it takes a longer time for the higher density and viscosity ratio case ($\dot{\gamma}t = 24.29$) to reach the steady state than the other case (steady state at $\dot{\gamma}t = 7.32$), as shown in the figure. From our simulations, we also report that the droplets for the case of higher density ratio and viscosity ratio (i.e., $\rho_{12} = 800$, $\mu_{12} = 60$) experience more oscillation before and after reaching the steady state.

To understand and unravel the underlying physics, we have plotted the magnitude of vorticity contours in Fig. 6. In addition, we define effective capillary ($\mathrm{Ca_{eff}} \equiv \frac{\mu_2 \dot{\gamma}_{\mathrm{eff}} R}{\sigma}$) and Reynolds ($\mathrm{Re_{eff}} \equiv \frac{\rho_2 \dot{\gamma}_{\mathrm{eff}} R^2}{\mu_2}$) numbers to account for the substantial distortion of the linear shear rate ($\dot{\gamma}_{\mathrm{eff}}$) due to the

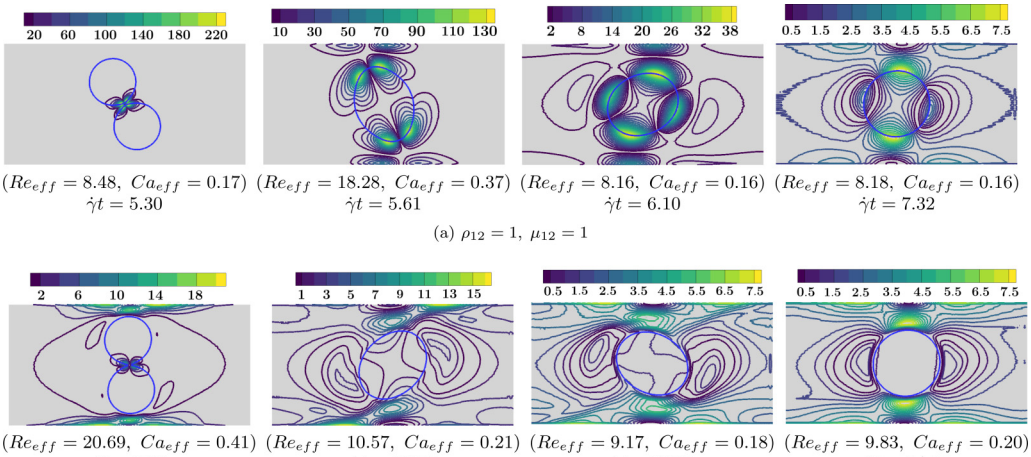

$(Re_{eff} = 8.48,\ Ca_{eff} = 0.17)$ $\dot{\gamma}t = 5.30$
$(Re_{eff} = 18.28,\ Ca_{eff} = 0.37)$ $\dot{\gamma}t = 5.61$
$(Re_{eff} = 8.16,\ Ca_{eff} = 0.16)$ $\dot{\gamma}t = 6.10$
$(Re_{eff} = 8.18,\ Ca_{eff} = 0.16)$ $\dot{\gamma}t = 7.32$

(a) $\rho_{12} = 1,\ \mu_{12} = 1$

$(Re_{eff} = 20.69,\ Ca_{eff} = 0.41)$ $\dot{\gamma}t = 9.39$
$(Re_{eff} = 10.57,\ Ca_{eff} = 0.21)$ $\dot{\gamma}t = 10.98$
$(Re_{eff} = 9.17,\ Ca_{eff} = 0.18)$ $\dot{\gamma}t = 12.20$
$(Re_{eff} = 9.83,\ Ca_{eff} = 0.20)$ $\dot{\gamma}t = 24.39$

(b) $\rho_{12} = 800,\ \mu_{12} = 60$

FIG. 6. Time-lapse images of induced vorticity (normalized by $\dot{\gamma} = 2U/H$) for the two marginal cases (a) $\rho_{12} = 1,\ \mu_{12} = 1$ and (b) $\rho_{12} = 800,\ \mu_{12} = 60$ with Re $= 1.0$, Ca $= 0.01$, We $= 0.01$, $\Delta X/2R = 1.26$, $\Delta Y/2R = 0.86$, and $2R/H = 0.39$. Four analytic snapshots for both of the cases from Fig. 5 are plotted here.

presence of the droplets. We, therefore, have adopted the approach in Ref. [41] to calculate the effective shear rate experienced by the droplets at each snapshot rather than assuming an imposed shear rate set directly by the input parameter.

For the case with the density ratio of $\rho_{12} = 1$ and viscosity ratio of $\mu_{12} = 1$ [Fig. 6(a), $\dot{\gamma}t = 5.30$], it can be observed that when the droplets approach each other, vorticities are generated at the region of the droplets' contact, which are due to the liquid bridge generated by the low pressure at the collision point. However, no vortical structures are found outside the droplets as the viscosity is the same for both droplets and the matrix fluid. The high-negative curvature of the liquid bridge formed at the beginning of coalescence leads to a prompt increase in the kinetic energy, thus helping generate the largest magnitude of vorticity when compared with other instances. On the other hand, for the case with the highest viscosity ratio and density ratio [Fig. 6(b), $\dot{\gamma}t = 9.39$], strong vortices are found not only in the contact region but also in regions near the wall. This is due to the interplay between shear stress and the curvature of the liquid bridge. It can also be seen that the amount and the magnitude of vortical structures near the wall region are higher than those in the contact region, making the droplets orient more in the flow direction during and after coalescence ($\dot{\gamma}t = 10.98$). The absence of such strong vortices near the wall region for the case with the unit density and viscosity ratio [Fig. 6(b)] allows the droplets to resist more against orienting in the flow direction during and after coalescence ($\dot{\gamma}t = 5.30$–5.61).

The reported values of $\mathrm{Re}_{\mathrm{eff}}$ experienced by the droplets for both marginal cases are larger than the value of $\mathrm{Re} = 1$ imposed by the input parameters. Such higher $\mathrm{Re}_{\mathrm{eff}}$ indicates the strong effect of the inertial force compared to the viscous force. This contribution of inertial force is even more significant for the higher-density-ratio case, especially during neck generation, which also dominates the surface tension force. As the droplet reaches the steady state, the contribution of inertia for the two density ratios is comparable. Additionally, increasing the density ratio (i.e., increasing the inertia of the droplets) induces higher oscillation of droplets during the progression to a steady state.

To measure the quality of such oscillation and quantify the time evolution of mutual displacement of droplets, we have plotted the evolution of dimensionless offset ($\Delta Y/2R$) as a function of the dimensionless horizontal position ($\Delta X/2R$) of the droplets, as shown in Fig. 7 for the marginal cases displayed in Fig. 5. Offset measurement (i.e., $\Delta X/2R$ and $\Delta Y/2R$) is taken by identifying the centers of both droplets, where the distance between them is calculated accordingly. When the droplets start to merge, some portion of their perimeter retains curvatures, as if they are part of a circle. In such instances, the horizontal and vertical offset positions are approximated based on the centers of curvature. From this representation, it is observed that initially, the droplets come closer to each other horizontally as well as vertically in both cases. For the case with $\rho_{12} = \mu_{12} = 1$, the coalescence occurs earlier than the case with a higher density ratio and viscosity ratio ($\rho_{12} = 800$, $\mu_{12} = 60$). This can be attributed to the lower inertia of the matrix fluid for density and viscosity ratio of unity (i.e., $\mathrm{Re}_{\mathrm{eff}} = 8.48$), which makes the droplets move faster during the flow, and the lower viscosity (i.e., $\mathrm{Ca}_{\mathrm{eff}} = 0.17$), which creates less resistance to their movement. In the case of higher ρ_{12} and μ_{12}, the top droplet passes over the bottom one due to higher inertia and the shear force created by the wall motion. At the same time, the droplets deform so that the liquid film entrapped between the droplets continues to drain out and gradually becomes thinner. At some point, the droplets come close enough to each other that the surface tension force becomes strong enough to start off the surface rupture and initiate the coalescence. During their coalescence, the droplets continue to rotate around each other and show small fluctuations before merging into a single steady-shaped droplet.

The evolution of the blue curve with the square markers ($\rho_{12} = 1$, $\mu_{12} = 1$) in Fig. 7 indicates that initially, the top droplet, being in the left position, continues to move in the right direction, passes the bottom droplet, and later returns toward the bottom droplet to coalesce and, finally, reach the steady shape. The black curve with circle marker ($\rho_{12} = 800$, $\mu_{12} = 60$) shows that their coalescence starts later than the case of $\rho_{12} = 1$, $\mu_{12} = 1$. In this case, when the droplets touch each other, the higher inertia slows down the motion of the top droplet rightwards, which can be noticed from the nature

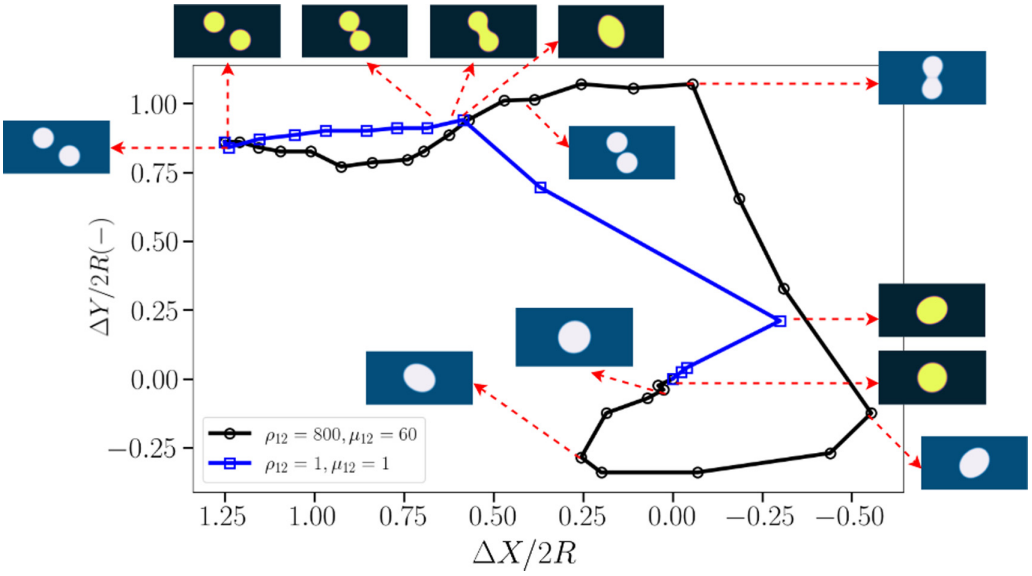

FIG. 7. Evolution of vertical offset as a function of horizontal distance between two droplets for the two extreme cases ($\rho_{12} = 1$, $\mu_{12} = 1$ and $\rho_{12} = 800$, $\mu_{12} = 60$) with Re $= 1.0$, Ca $= 0.01$, We $= 0.01$, $\Delta X/2R = 1.26$, $\Delta Y/2R = 0.86$, and $2R/H = 0.39$. The snapshots from Fig. 5 have been depicted here and their locations have been marked with red dashed arrow.

of the black curve trajectory. Also, the black curve follows a circular path near the end, revealing the rotation of droplets around each other before reaching a steady state.

From the analysis discussed above, we have observed that the two extreme cases of density and viscosity ratios have crucial roles in the droplet's motion and coalescence behavior. To investigate the role that varying density ratios and viscosity ratios can have on the behavior of offset trajectories, we have simulated three cases with different density ratios ($\rho_{12} = 60, 430, 800$) while keeping the viscosity ratio fixed ($\mu_{12} = 60$) and three cases with different viscosity ratios ($\mu_{12} = 24, 36, 60$) maintaining a fixed density ratio ($\rho_{12} = 800$) and plotted their offset trajectory in Fig. 8. Looking at the results of Fig. 8(a), it can be noticed from the change of $\Delta X/2R$ that

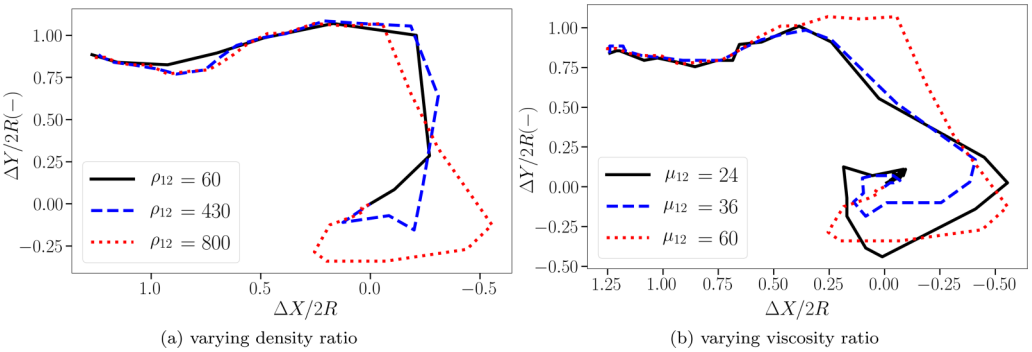

(a) varying density ratio (b) varying viscosity ratio

FIG. 8. Effect of different density ratios (left) keeping the viscosity ratio fixed ($\mu_{12} = 60$) and different viscosity ratios (right) with a fixed density ratio ($\rho_{12} = 800$) on the evolution of both horizontal and vertical offset. All the six simulations were conducted with Ca $= 0.01$, Re $= 1.0$, We $= 0.01$, $\Delta X/2R = 1.26$, $\Delta Y/2R = 0.86$, and $2R/H = 0.39$.

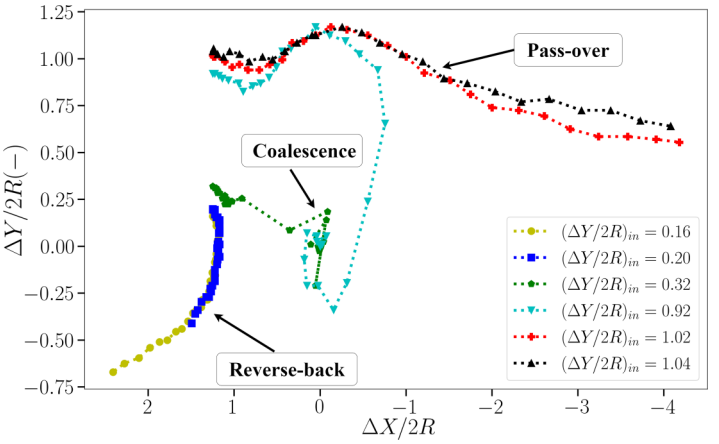

FIG. 9. Effect of initial offset ($\Delta Y/2R_{\text{in}}$) on coalescence for the case with $\rho_{12} = 800$, $\mu_{12} = 60$, Ca $= 0.01$, Re $= 1.0$, We $= 0.01$, $\Delta X/2R = 1.26$, and $2R/H = 0.39$.

for the lower density ratio ($\rho_{12} = 60$), droplets approach the collision state faster and coalesce without getting away from each other. On the other hand, for the highest-density-ratio case ($\rho_{12} = 800$), droplets move slowly toward each other and continue to move further away than in the other two cases. This slow movement of droplets is due to the high inertia of droplets, which causes a circulating trajectory and oscillation before merging (i.e., $\Delta X/2R = 0$) into a single droplet.

For the cases with different viscosity ratios demonstrated in Fig. 8(b), there is not a significant difference to be observed initially. The impact of viscosity difference comes into effect as soon as the droplets start approaching each other, displaying different morphology and deformation behavior. Small viscosity ratio allows the droplets to deform substantially, whereas a large viscosity ratio tends to prevent it. For a low viscosity ratio ($\mu_{12} = 24$), the two droplets oscillate for a significant amount of time along with a swirling motion before reaching a steady state. Taken together, increasing the viscosity ratio plays an appreciable role in retaining droplets' shape and thus impedes the undulation as found for the case with $\mu_{12} = 60$.

C. The joint effect of initial offset, density ratio, and viscosity ratio

The initial offset between droplets $(\Delta Y/2R)_{\text{in}}$ has been detected to be a crucial parameter that significantly impacts the coalescence mode in previous studies, as discussed in Sec. I. Here we investigate the interplay among initial offset, inertial force, and viscous force on the trajectories and collision modes of droplet pairs, which has not been addressed in prior investigations. To begin with, the evolution of the vertical offset as a function of the horizontal distance for different initial vertical offsets [$(\Delta Y/2R)_{\text{in}} = 0.16$, 0.20, 0.32, 0.92, 1.02, and 1.04], while keeping $\rho_{12}(= 800)$ and $\mu_{12}(= 60)$ fixed, has been illustrated in Fig. 9. The droplets pass over each other for a higher initial offset value, whereas they reverse their trajectory when the value of $(\Delta Y/2R)_{\text{in}}$ is relatively smaller. Additionally, the coalescence mode of droplet pairs has been observed for the range of $(\Delta Y/2R)_{\text{in}}$ between two critical initial offsets. Collectively, this plot indicates the existence of three collision modes that are functions of initial offsets and defines those three regions separated by the lower and higher critical initial offsets, which is in agreement with previous studies for $\rho_{12} = 1$ and $\mu_{12} = 1$ [18,19].

We have constructed phase diagrams (Fig. 10) that allow us to critically investigate regions of different collision modes based on the combined effects of density ratio, viscosity ratio, and initial offset. Figure 10(a) presents the phase diagram of the collision modes in the effect of different

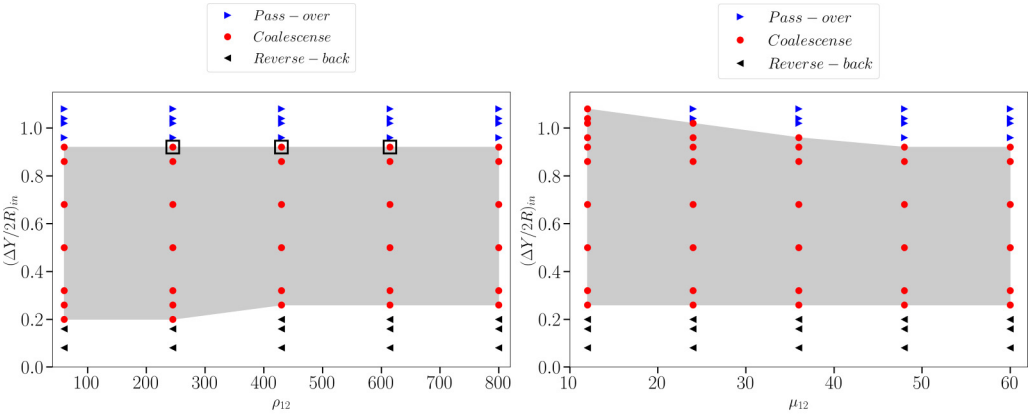

(a) Initial offset vs Density ratio ($\mu_{12} = 60$) (b) Initial offset vs Viscosity ratio ($\rho_{12} = 800$)

FIG. 10. Phase diagrams to show different regions of collision modes for varying initial offsets with (a) different density ratios and (b) different viscosity ratios with Ca = 0.01, Re = 1.0, We = 0.01, $\Delta X/2R = 1.26$, $2R/H = 0.39$. The right-pointing triangles indicate pass-over cases, the circles present the coalescence, and the left-pointing triangles are the cases where the droplets reverse their trajectory instead of coalescing. The coalescence region is shaded in gray for the clarity of visualization and to distinguish the different regions properly.

initial offsets [$(\Delta Y/2R)_{\text{in}} = 0.08, 0.16, 0.20, 0.26, 0.32, 0.50, 0.68,$ 0.86, 0.92, 0, 96, 1.02, 1.04, and 1.08] and density ratios ($\rho_{12} = 60, 245, 430, 615,$ and 800), keeping the viscosity ratio fixed ($\mu_{12} = 60$). The reverse-back and pass-over motions occur at smaller and larger initial offsets, respectively, while the coalescence mode is observed at an intermediate initial offset. Consistent with previous studies [18,19], for a given density ratio, increasing the initial offset may change the droplets' motion from reverse-back to coalescence and to pass-over modes. The critical value of the initial offset above which the pass-over motion occurs is observed around $(\Delta Y/2R)_{\text{in}} = 0.96$, independent of the density ratio. However, the reverse-back mode shows dependency on both the initial offset and the density ratio. As a result of this combined effect, the critical initial offset below which the reverse-back mode occurs increases with the increase in density ratio. This results in the existence of not only an upper critical initial offset, below which the coalescence mode occurs, but also a lower critical initial offset, above which droplets coalesce in an inertia-dependent manner. During the approach of the droplets, they encounter a film of matrix fluid between them. The thickness of the film decreases as the distance between the pair droplets decreases, resulting in film drainage. When the initial offset is too large [i.e., $(\Delta Y/2R)_{\text{in}} \geqslant 0.96$], the time for the film drainage is not enough, and the droplets pass over each other, no matter how large the density ratio is. When the initial offset is relatively small, the vertical distance between the droplets decreases during their approach until they locate precisely at the same elevation. This results in reverse-back motions of droplets without passing over each other. When the initial offset of droplets is between the upper and lower critical limits, the droplets approach each other and start passing over each other. During the pass-over motion of the droplets, the matrix film between the droplet interfaces gets drained and sufficiently thinned, resulting in the rupture of the film and eventual coalescence of the droplets. Increasing the density ratio for the motion of pair droplets at relatively small values of initial offset results in a stronger inertial force that slows down the film drainage rate and increases the value of the critical initial offset. For the initial offset of $(\Delta Y/2R)_{\text{in}} = 0.92$, shown in Fig. 10(a), three cases are marked with square markers as they show some unusual course of motion during the evolution of coalescence and will be discussed with in-detail analysis later in this section. A similar phase diagram on the effect of initial offset but for different viscosity ratios has been demonstrated in Fig. 10(b). It is clear that the reverse-back motion occurs for the initial offset below

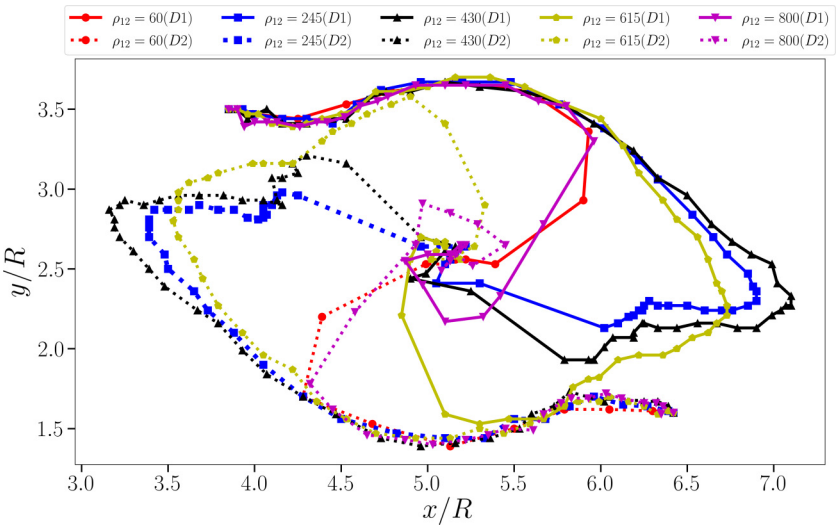

FIG. 11. Trajectory of both droplets for the critical case of $(\Delta Y/2R)_{\text{in}} = 0.92$ throughout the evolution with varying density ratio and for Ca = 0.01, Re = 1.0, We = 0.01, $\Delta X/2R = 1.26$, and $2R/H = 0.39$. The solid line (D1) curve represents droplet-1 (top droplet) motion and the dotted line (D2) curve indicates the motion of droplet-2 (bottom droplet).

$[(\Delta Y/2R)_{\text{in}} = 0.20]$, where the variation of viscosity ratio does not affect the lower critical offset. In contrast, the upper critical initial offset, where the transition from coalescence to pass-over mode occurs, shows a dependency on the viscosity ratio variation. With increasing the viscosity ratio, the mobility of the interface is lowered, which hinders film drainage. As a result, the upper critical initial offset below which the coalescence occurs decreases. The smallest viscosity ratio considered in this study ($\mu_{12} = 12$) induces the largest mobility and deformation of the droplets, which results in the coalescence of droplets even at the highest upper critical initial offset $[(\Delta Y/2R)_{\text{in}} = 1.08]$.

Interestingly, we observed that even though the motion of droplets under pairwise interactions at upper critical initial offset $[(\Delta Y/2R)_{\text{in}} = 0.92]$ leads to the coalescence mode, their evolution during the approach and rotation over each other is dramatically influenced by the change in the density ratio. We marked those special cases with square symbols in Fig. 10(a). To clarify this further, Figs. 11 and 12 show the instantaneous movement trajectories of both droplets and their relative trajectories, respectively, for different density ratios at $(\Delta Y/2R)_{\text{in}} = 0.92$. For the collision of droplet pairs under varying density ratios, there is a competition between shear forces pulling the upper left droplet over the lower right droplet and inertia force pulling the upper left droplet down. with increasing the density ratio, due to the higher inertia of the droplets, they would slowly go through the pathline of the main flow; the higher the density ratio, the larger the deviation from the carrying flow pathline. An important point that should be considered is that the walls' presence significantly influences droplets' evolution and deformation at a relatively high initial offset. This increases the pressure between them, forcing the droplets to move away from the walls. Owing to these competing terms, the droplets may rotate over each other for a longer time before contact. For the same reason, there is no apparent systematic trend in how the evolution of droplets during the approach depends on the change in density ratio.

At a density ratio of 60, the high inertia of the surrounding flow pushes the droplets toward each other during their rotational motion. This high hydrodynamic force increases the film drainage rate, and consequently, the droplets coalesce on their first approach, as can be seen in Figs. 11 and 12. At a density ratio of 800, the droplets behave like very heavy solid spheres with more resistance against deformation. Generally, by increasing the density ratio, there would be a difference between the

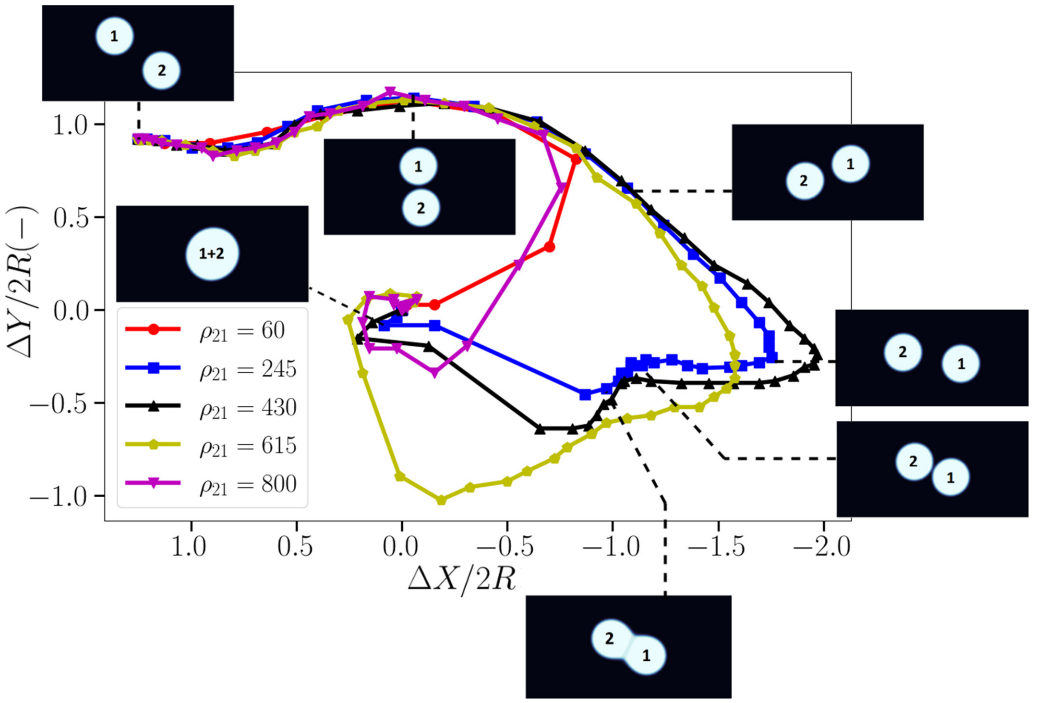

FIG. 12. Evolution of vertical offset as a function of horizontal distance of the droplets for varying density ratio with $(\Delta Y/2R)_{\text{in}} = 0.92$ while the other parameter values are kept fixed. Snapshots of some critical instants for the case of $\rho_{12} = 245$ are appended and their exact locations are pointed with the dashed line.

droplet's speed and the main flow velocity. As a result, the relative velocity difference for the density ratio of 800 is fairly high, which enhances the motion of droplets from the wall and forces them to coalesce in a shorter period of time. At intermediate values of density ratio (i.e., $\rho_{12} = 245$–615), inertia forces compete strongly with shear forces, which can even offset each other. The consequence of this competition is an intensive deviation of the droplets' motion from the main flow streamline, forcing them to rotate over each other for a longer period of time before having contact.

D. The joint effect of confinement, initial offset, density ratio, and viscosity ratio

Besides the initial offset, the confinement also affects the motion and behavior of pairwise interactions between droplets in the confined shear flow. Figure 13 shows the evolution of the vertical offset as a function of the horizontal distance between the droplets for different confinement ratios $(2R/H)$ while keeping all other parameters, including initial offset $(\Delta Y/2R)_{\text{in}} = 0.86$), density ratio ($\rho_{12} = 800$), and viscosity ratio ($\mu_{12} = 60$), fixed.

For the lowest confinement ratio case ($2R/H = 0.30$), the curve shows the pass-over motion of droplets during their pairwise interactions. As the gap between the walls decreases (i.e., the confinement ratio increases), the motion of the droplets transits from pass-over to coalescence mode. Thus, in line with previous studies [18,19], confinement can promote coalescence. The behavior of droplets for the pass-over motion requires them to approach and rotate over each other with adequate spacing from each other and from the walls to avoid their coalescence. Therefore, the droplets cannot make such contact to coalesce for the lowest confinement ratio. Instead, they start to move in the reverse direction to adjust the shear drag of the flow from the opposite direction.

However, the role of the geometrical confinement on the collision mode can be significantly affected by the initial offset of the droplets, owing to the change in the gap between the droplets

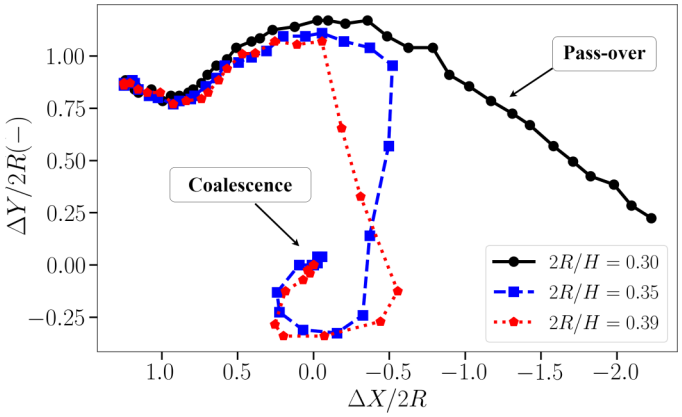

FIG. 13. Evolution of vertical offset as a function of horizontal distance between two droplets for three different confinement ratio $2R/H$ cases with $(\Delta Y/2R)_{\text{in}} = 0.86$, $\rho_{12} = 800$, $\mu_{12} = 60$, Ca $= 0.01$, Re $= 1.0$, and We $= 0.01$.

and the walls. The results in Sec. III C revealed the importance of the inertia and viscous forces combined with the initial offset on the evolution of droplets and the transition of collision modes. How collaborative effects of confinement ratio, initial offset, density ratio, and viscosity ratio affect the trajectories and collision modes of interacting droplets have not been explored and quantified. Hence the simulations with varying all the above-mentioned parameters were performed to find the transition of collision mode and presented as phase diagrams in Fig. 14. An argument based on extreme values of density ratio and viscosity ratio allows the construction of three phase diagrams, as shown in Fig. 14 for (a) $\rho_{12} = 60$, $\mu_{12} = 60$, (b) $\rho_{12} = 800$, $\mu_{12} = 60$, and (c) $\rho_{12} = 800$, $\mu_{12} = 24$. Increasing the confinement ratio for a given density and viscosity ratio generally induces a higher critical initial offset for the transition from reverse-back to coalescence or from coalescence to the pass-over motion of droplets. Previous studies for the density and viscosity ratios of unity also support our finding that the critical initial offset boundary increases with the confinement ratio [18,19]. However, it is also clear from Figs. 14(a)–14(c) that changing the density ratio and viscosity ratio can significantly affect the interplay between critical initial offset and critical confinement on the collision mode of droplets.

From Fig. 14(a), which is for density ratio of $\rho_{12} = 60$ and viscosity ratio of $\mu_{12} = 60$, it can be observed that the lowest confinement ratio ($2R/H = 0.30$) initiates pass-over phenomena for initial offset $(\Delta Y/2R)_{\text{in}}$ as low as 0.86. In contrast, the pass-over motion for other confinement ratios starts at $(\Delta Y/2R)_{\text{in}} = 0.96$. On the contrary, from the lower region of the same figure, it can clearly be noticed that the higher confinement ratio promotes the reverse-back motion of droplets. It is also found that the droplets for the confinement ratio of $2R/H = 0.39$ reverse their movement direction instead of coalescing up to the initial offset of $(\Delta Y/2R)_{\text{in}} = 0.16$, while droplets for the confinement ratios of $2R/H = 0.30$ and 0.33, coalesce with the minimum initial offset $[(\Delta Y/2R)_{\text{in}} = 0.04]$ considered here.

Looking at Fig. 14(b), which is for the largest density ratio ($\rho_{12} = 800$) and viscosity ratio ($\mu_{12} = 60$), it can be noticed that the general trends for the transition from reverse-back to coalescence to pass-over modes concerning confinement ratio are similar to the case with the lowest density ratio ($\rho_{12} = 60$). However, the pass-over motion starts to happen with a smaller initial offset of $(\Delta Y/2R)_{\text{in}} = 0.68$ for the lowest confinement ($2R/H = 0.30$), and with the increase of confinement, this critical point of initial offset increases. On the lower extreme of the initial offset, larger confinement favors reverse-back motions, and for the largest confinement ($2R/H = 0.39$), droplets turn back to their reversed trajectory even up to the initial offset of $(\Delta Y/2R)_{\text{in}} = 0.20$.

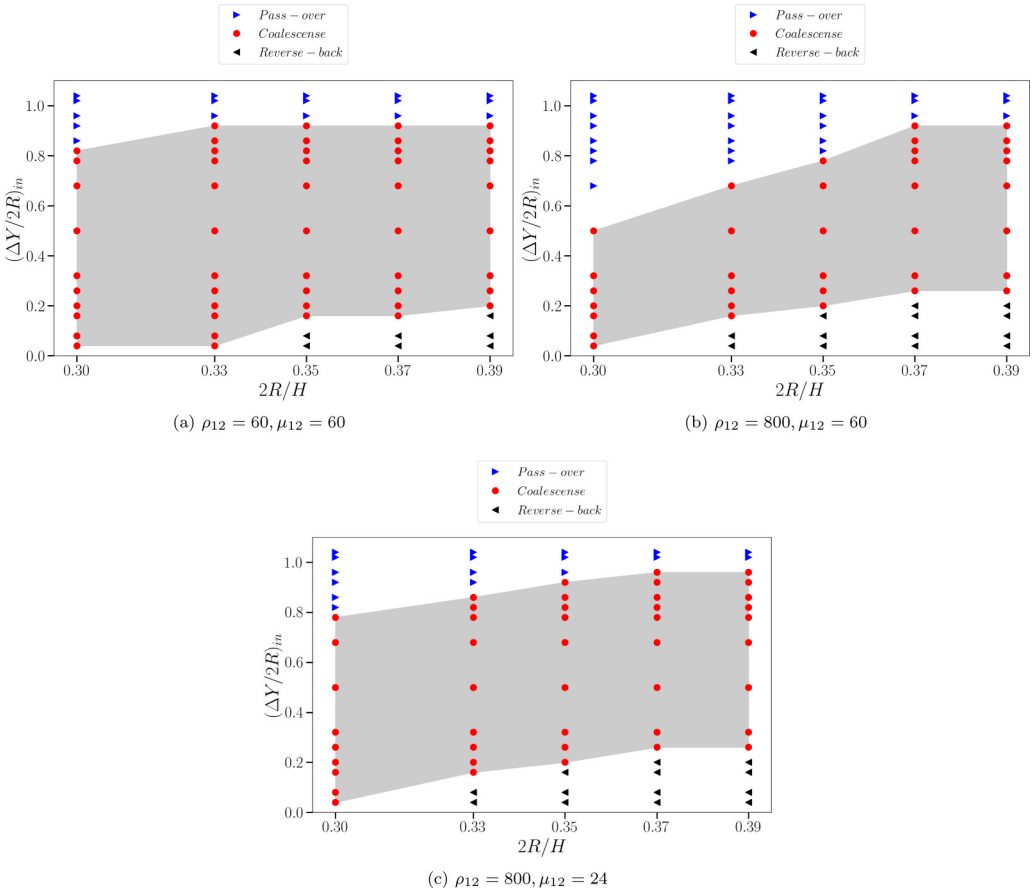

(a) $\rho_{12} = 60, \mu_{12} = 60$

(b) $\rho_{12} = 800, \mu_{12} = 60$

(c) $\rho_{12} = 800, \mu_{12} = 24$

FIG. 14. Phase diagrams of collision mode for pairwise interaction of droplets with different initial offset, confinement ratio, density ratio, and viscosity ratio.

The results of Figs. 14(a) and 14(b) suggest that even though the general trend for the transition mode of droplets as a function of density ratio is the same, the coalescence region is narrowed down in the case of higher density ratio ($\rho_{12} = 800$), which is one of the crucial findings of this study. With an increasing density ratio, coalescence becomes more difficult as the mobility of the interface is lower, resulting in inconvenient film drainage. Additionally, at higher density ratios, the interface of droplets experiences higher shear stress, which increases the tendency of the droplets to be pulled over each other. This results in a smaller critical initial offset for the upper boundary when the confinement ratio is less than 0.37, as well as a larger critical initial offset for the lower boundary when the confinement ratio is higher than 0.33.

Figures 14(b) and 14(c) compare the collision mode of interacting droplets and their boundary for systems with the lowest [Fig. 14(c)] and highest viscosity ratios [Fig. 14(b)]. Similarly, the region for the coalescence motion is narrowed down when the viscosity ratio is increased. However, it can be observed that both figures for the reverse-back region share the same outcomes. The difference can be noticed in the boundary between coalescence and pass-over regions, especially for low to intermediate values of the confinement ratio considered here. As the viscosity ratio increases from 24 to 60, the critical upper initial offset above which pass-over motion occurs decreases, and lowering the confinement ratio further decreases this critical offset boundary. Similarly to the effect of the density ratio, increasing the viscosity ratio could also make the coalescence more strenuous.

In fact, the droplets with a larger viscosity ratio have a greater tendency to be pulled along with the rotation of the second droplet. This results in stronger hydrodynamic interactions between droplets and suppression of coalescence, especially when the confinement ratio decreases.

IV. CONCLUSION

This work simulates the coalescence of equal-sized droplet pairs in a confined shear flow using the free-energy-based binary-liquid lattice Boltzmann method. The effect of various physical and geometric parameters on the coalescence dynamics and their outcomes have been systematically examined and analyzed. Particularly, we attempted to (i) understand the relative influence of density ratios and viscosity ratios on the morphology of droplets and their coalescence behavior throughout the evolution, (ii) explore the effect of wall confinement and initial vertical offset between droplets on collision modes, and (iii) examine the combined effect of the aforementioned parameters on the collision outcome.

Simulations with different density ratios and viscosity ratios reveal that the interaction between viscous and inertia forces plays a vital role in the coalescence nature of droplets, their deformation, course of trajectory, as well as their expedition toward the steady state. An increase in density ratio results in a slow movement of droplets, requiring a longer time for their hydrodynamic interactions. Although the change in viscosity ratio does not bring about significant variation in coalescence timing, it has a considerable impact on the droplets' deformation. With the increase in viscosity ratio, droplets' deformation and oscillation tend to decrease during coalescence, affecting their course trajectory substantially.

Second, we tried exploring the effect of the initial vertical offset of droplets $[(\Delta Y/2R)_{\text{in}}]$ while keeping all other parameters fixed and found three regions separated by the lower and higher critical initial offsets. There has been an upper critical initial offset, above which the droplets pass over, and a lower critical initial offset, below which the droplets reverse their trajectory instead of following the sheared direction. The coalescence mode of pair droplets has been observed in the region between those two critical offsets. Additionally, we have observed that even though the motion of droplets at an upper critical initial offset leads to the coalescence mode, their evolution during the approach and rotation over each other is dramatically influenced by the change in the density ratio. This can be explained by the fact that the motion and deformation of droplets at a relatively high initial offset would be more affected by the pressure increase between droplets and walls, forcing them to move away from the walls. On the other hand, at intermediate values of density ratio (i.e., $\rho_{12} = 245$–615), inertia forces compete strongly with shear forces, which can even offset each other. The consequence of this competition is an intensive deviation of the droplets' motion from the main flow streamline, forcing them to rotate over each other for a more extended period of time before having contact. Besides the initial offset, the confinement ratio $(2R/H)$ also affects the motion and behavior of pairwise interactions between droplets in the confined shear flow. Higher confinement has always been supportive of the coalescence of the droplets, whereas lower confinement induces convenient spacing between the droplets and the walls, thus providing a favorable environment for them to pass over. Nevertheless, we emphasize that the stated conclusion about the confinement effect on the collision outcome is always responsive to the other parameters (e.g., Re, Ca, and size of droplets).

Finally, we have assembled the combined effects of vertical initial offset, confinement, density ratios, and viscosity ratios into phase diagrams. Depending on the initial offset, three separate regions for three different collision modes (pass-over, coalescence, and reverse-back) can be defined, where the span of those regions is highly sensitive to density ratio and viscosity ratio, in addition to confinement. Particularly, the interaction of pair droplets under low confinement and low initial offset leads to coalescence, and not a single case with a reverse-back mode has been found. However, higher confinement with a lower initial offset generally provides a favorable environment for droplets to reverse their trajectories, and the pass-over motion always happens above a specific critical value of the initial offset. Additionally, a careful observation discloses that the higher value

of density and viscosity ratios shrinks the region of the coalescence mode and assists in increasing the number of pass-over cases along with reverse-back cases, depending on the initial offset and confinement. In contrast, the lower density and viscosity ratios give rise to a broader region of coalescence mode in the phase diagrams.

[1] J. Xu, P. Cheng, and T. Zhao, Gas–liquid two-phase flow regimes in rectangular channels with mini/micro gaps, Int. J. Multiphase Flow **25**, 411 (1999).

[2] T. Zhao and Q. Bi, Co-current air–water two-phase flow patterns in vertical triangular microchannels, Int. J. Multiphase Flow **27**, 765 (2001).

[3] Y. Zhao, H. C. Shum, L. L. Adams, B. Sun, C. Holtze, Z. Gu, and D. A. Weitz, Enhanced encapsulation of actives in self-sealing microcapsules by precipitation in capsule shells, Langmuir **27**, 13988 (2011).

[4] I. Halliday, R. Law, C. M. Care, and A. Hollis, Improved simulation of drop dynamics in a shear flow at low reynolds and capillary number, Phys. Rev. E **73**, 056708 (2006).

[5] A. K. Haghighat, M. G. Olsen, R. D. Vigil, and A. Sarkar, Droplet coalescence and phase separation in a topical ointment: Effects of fluid shear and temperature, Int. J. Pharmaceut. **591**, 119872 (2020).

[6] H. Tokumitsu, H. Ichikawa, Y. Fukumori, and L. H. Block, Preparation of gadopentetic acid-loaded chitosan microparticles for gadolinium neutron-capture therapy of cancer by a novel emulsion-droplet coalescence technique, Chem. Pharm. Bull. **47**, 838 (1999).

[7] Y.-J. Zhao, X.-W. Zhao, J. Hu, J. Li, W.-Y. Xu, and Z.-Z. Gu, Multiplex label-free detection of biomolecules with an imprinted suspension array, Angew. Chem., Int. Ed. **48**, 7350 (2009).

[8] Y. Zhao, Z. Xie, H. Gu, C. Zhu, and Z. Gu, Bio-inspired variable structural color materials, Chem. Soc. Rev. **41**, 3297 (2012).

[9] J.-J. Elmendrop and A.-K. Van Der Vegt, A study on polymer blending microrheology: Part IV. The influence of coalescence on blend morphology origination, Polymer Engineering & Science, **26**, 1332 (1986).

[10] M. Minale, J. Mewis, and P. Moldenaers, Study of the morphological hysteresis in immiscible polymer blends, AIChE J. **44**, 943 (1998).

[11] A. Ramic, S. Hudson, A. Jamieson, and I. Manas-Zloczower, Temporary droplet-size hysteresis in immiscible polymer blends, Polymer **41**, 6263 (2000).

[12] L. Nilsson and B. Bergenståhl, Adsorption of hydrophobically modified starch at oil/water interfaces during emulsification, Langmuir **22**, 8770 (2006).

[13] L. Lobo and A. Svereika, Coalescence during emulsification, J. Colloid Interface Sci. **261**, 498 (2003).

[14] S. M. Jafari, E. Assadpoor, Y. He, and B. Bhandari, Re-coalescence of emulsion droplets during high-energy emulsification, Food Hydrocoll. **22**, 1191 (2008).

[15] D. Wasan, S. Shah, N. Aderangi, M. Chan, and J. McNamara, Observations on the coalescence behavior of oil droplets and emulsion stability in enhanced oil recovery, Soc. Pet. Eng. J. **18**, 409 (1978).

[16] D. Wasan, J. McNamara, S. Shah, K. Sampath, and N. Aderangi, The role of coalescence phenomena and interfacial rheological properties in enhanced oil recovery: An overview, J. Rheol. **23**, 181 (1979).

[17] A.-K. Chesters, The modeling of coalescence processes in fluid-liquid dispersions: A review of current understanding, Chemical Engineering Research and Design: transactions of the Institution of Chemical Engineers: Part A **69**, 259 (1991).

[18] P. De Bruyn, R. Cardinaels, and P. Moldenaers, The effect of geometrical confinement on coalescence efficiency of droplet pairs in shear flow, J. Colloid Interface Sci. **409**, 183 (2013).

[19] P. De Bruyn, D. Chen, P. Moldenaers, and R. Cardinaels, The effects of geometrical confinement and viscosity ratio on the coalescence of droplet pairs in shear flow, J. Rheol. **58**, 1955 (2014).

[20] S. Guido and M. Simeone, Binary collision of drops in simple shear flow by computer-assisted video optical microscopy, J. Fluid Mech. **357**, 1 (1998).

[21] O. Shardt, J. Derksen, and S. K. Mitra, Simulations of droplet coalescence in simple shear flow, Langmuir **29**, 6201 (2013).

[22] B. Huang, H. Liang, and J. Xu, Lattice Boltzmann simulation of binary three-dimensional droplet coalescence in a confined shear flow, Phys. Fluids **34**, 032101 (2022).
[23] D. Chen, R. Cardinaels, and P. Moldenaers, Effect of confinement on droplet coalescence in shear flow, Langmuir **25**, 12885 (2009).
[24] Y. Chen and C. Wang, Hydrodynamic interaction of two deformable drops in confined shear flow, Phys. Rev. E **90**, 033010 (2014).
[25] K. Sarkar and R. K. Singh, Spatial ordering due to hydrodynamic interactions between a pair of colliding drops in a confined shear, Phys. Fluids **25**, 051702 (2013).
[26] M. Bayareh and S. Mortazavi, Binary collision of drops in simple shear flow at finite reynolds numbers: Geometry and viscosity ratio effects, Adv. Eng. Softw. **42**, 604 (2011).
[27] M. Loewenberg and E. Hinch, Collision of two deformable drops in shear flow, J. Fluid Mech. **338**, 299 (1997).
[28] T. Lee and L. Liu, Lattice Boltzmann simulations of micron-scale drop impact on dry surfaces, J. Comput. Phys. **229**, 8045 (2010).
[29] T. Lee, Effects of incompressibility on the elimination of parasitic currents in the lattice Boltzmann equation method for binary fluids, Comput. Math. Appl. **58**, 987 (2009).
[30] S. Farokhirad, J. F. Morris, and T. Lee, Coalescence-induced jumping of droplet: Inertia and viscosity effects, Phys. Fluids **27**, 102102 (2015).
[31] R. Zhang, S. Farokhirad, T. Lee, and J. Koplik, Multiscale liquid drop impact on wettable and textured surfaces, Phys. Fluids **26**, 082003 (2014).
[32] S. Farokhirad and T. Lee, Computational study of microparticle effect on self-propelled jumping of droplets from superhydrophobic substrates, Int. J. Multiphase Flow **95**, 220 (2017).
[33] S. Farokhirad, M. Mohammadi Shad, and T. Lee, Coalescence-induced jumping of immersed and suspended droplets on microstructured substrates, Eur. J. Comput. Mech. **26**, 205 (2017).
[34] A. Mohamad, *Lattice Boltzmann Method*, Vol. 70 (Springer, Berlin, 2011).
[35] P. L. Bhatnagar, E. P. Gross, and M. Krook, A model for collision processes in gases. i. small amplitude processes in charged and neutral one-component systems, Phys. Rev. **94**, 511 (1954).
[36] X. He, X. Shan, and G. D. Doolen, Discrete Boltzmann equation model for nonideal gases, Phys. Rev. E **57**, R13(R) (1998).
[37] D. Lee, J.-Y. Huh, D. Jeong, J. Shin, A. Yun, and J. Kim, Physical, mathematical, and numerical derivations of the cahn–hilliard equation, Comput. Mater. Sci. **81**, 216 (2014).
[38] P. Yue, C. Zhou, and J. Feng, Sharp-interface limit of the cahn–hilliard model for moving contact lines, J. Fluid Mech. **645**, 279 (2010).
[39] P. Yue and J. Feng, Can diffuse-interface models quantitatively describe moving contact lines? Eur. Phys. J. Spec. Top. **197**, 37 (2011).
[40] D. Jacqmin, Calculation of two-phase navier–stokes flows using phase-field modeling, J. Comput. Phys. **155**, 96 (1999).
[41] S. Frijters, F. Günther, and J. Harting, Effects of nanoparticles and surfactant on droplets in shear flow, Soft Matter **8**, 6542 (2012).